Indian Journal of Engineering & Materials Sciences
Vol. 4, April 1997, pp. 41-48

Computation of aerodynamic load and coefficient for satellite launch vehicle

R C Mehta* & M S Sastry
Aerodynamics Division, Vikram Sarabhai Space Centre, Trivandrum 695 022, India

Received 13 May 1996; accepted 20 November 1996

The time-dependent compressible, axisymmetric Euler equations are solved using fifth stage Runge-Kutta time-stepping method to obtain flow field over a typical heat shield of the satellite launch vehicle. The local normal load distributions, normal force coefficient and centre of pressure are calculated using tangent-cone method in conjunction with the numerically computed pressure variation. The present hybrid scheme can be easily employed to obtain preliminary design of the heat shield before it can be simulated in the wind-tunnel facility. Numerical results of the present analysis are compared with the available experimental data, and found in good agreement between them.

A blunt shaped forebody of the launch vehicle is generally designed to reduce aerodynamic heating rate whereas the bulbous shaped payload shroud is selected to accommodate increases in payload volume of the satellite. The estimation of flow field characteristics around such a body configuration is of considerable practical, as well as research interest. Moreover, the knowledge of the normal load distribution and aerodynamic coefficient is required for structural design of the satellite launch vehicle.

Currently applicable numerical algorithms to compute the compressible flow about satellite launch vehicle are three-dimensional inviscid or viscous analysis. But the numerical solution of the three-dimensional Euler or Navier-Stokes equations demands excessive computer time and memory. Therefore, fluid dynamicists have looked for simple methods to estimate aerodynamic force and coefficient at high speed regimes. Numerous methods are available for predicting the pressure coefficients on circular cone at angle of attack[1,2]. McBrayer[3] has employed empirical correlation plots to compute pressure distribution about yawed cones and ogives at Mach numbers from 1.25 to 3.0. A correlation[4] of the pressure distribution is available over a blunted slender cone at various angles of incidence by using the tangent-cone method. They determined normal force coefficient from the measured circumferential pressure distribution at angle of attack and compared with the prediction by tangent-cone method applied to the emperical zero lift pressure correlation. The circumferencial pressure distribution using the tangent-cone method[5] has been computed previously for a typcial launch vehicle which is having spherical shaped cap followed with cone, cylinder and forward facing ramp.

With the advances in Computational Fluid Dynamics, the aerodynamic force and coefficient can be computed over the launch vehicle by solving compressible inviscid equations. The three-dimensional numerical solution of the Euler equations demands larger computing facility in terms of computer memory and CPU time. In the present paper, a hybrid method is developed for the aerodynamic design of the heat shield in order to reduce the necessity of the larger computer facility. Moreover, the present method will reduce the numbers of blow-down of the wind-tunnel for selecting the final heat shield configuration. In the present paper, the flow field is computed by solving numerically the axisymmetric Euler equations using finite volume technique. The circumferential pressure distribution is obtained using the tangent-cone method in conjunction with the numerical analysis. The present numerical algorithm is simple and can easily be implemented on an IBM work station to compute the flow field as well as local normal load variation, and aerodynamic coefficient.

Governing Equations

The equations solved are the axisymmetric Euler equations describing the flow of an inviscid, compressible fluid. The governing equations are

*For correspondence.

written to conservation form as:

$$\frac{\partial \mathbf{U}}{\partial t}+\frac{\partial \mathbf{F}}{\partial x}+\frac{1}{r}\frac{\partial (r\mathbf{G})}{\partial r}+\frac{\mathbf{H}}{r}=0 \qquad \ldots (1)$$

where

$$\mathbf{U}=\begin{vmatrix}\rho\\ \rho u\\ \rho v\\ \rho e\end{vmatrix},\quad \mathbf{F}=\begin{vmatrix}\rho u\\ \rho u^2+p\\ \rho vu\\ (\rho e+p)u\end{vmatrix},\quad \mathbf{G}=\begin{vmatrix}\rho v\\ \rho uv\\ \rho v^2+p\\ (\rho e+p)v\end{vmatrix}$$

$$\mathbf{H}=\begin{vmatrix}0\\ 0\\ p\\ 0\end{vmatrix} \qquad \ldots (2)$$

The specific total energy e is defined relative to the specific energy E and fluid velocity components by

$$e=E+\frac{1}{2}(u^2+v^2) \qquad \ldots (3)$$

Finally, an equation of state is specified to relate the flow variables to the static pressure as

$$p=\rho E(\gamma-1) \qquad \ldots (4)$$

Numerical Formulations

An integral form of Eq. (1), over a finite volume fixed in time is:

$$r_c\frac{\partial}{\partial t}\int_{\Omega}\mathbf{U}\,d\Omega+\int_{\Gamma}\bar{r}(\mathbf{F}\,dr-\mathbf{G}\,dx)+\int_{\Omega}\mathbf{H}\,d\Omega=0 \qquad \ldots (5)$$

where Ω refers to the volume with boundary Γ, r_c is the centroid of the cell and $\bar{r}$ is the average cell radius. The computational domain is divided into a finite number of quadrilateral cells. The conservative variables within each cell are calculated by their average value at the cell centre and such quantities are denoted by suffix (i,j). A system of ordinary differential equations have been obtained by applying Eq. (5) separately to each cell. These equations have the form:

$$r_c\Delta A_{i,j}\frac{d(\mathbf{U}_{ij})}{dt}+\mathbf{Q}(\mathbf{U}_{ij})+r_c\Delta A_{ij}\,\mathbf{H}(\mathbf{U}_{ij})+\mathbf{D}(\mathbf{U}_{ij})=0 \qquad \ldots (6)$$

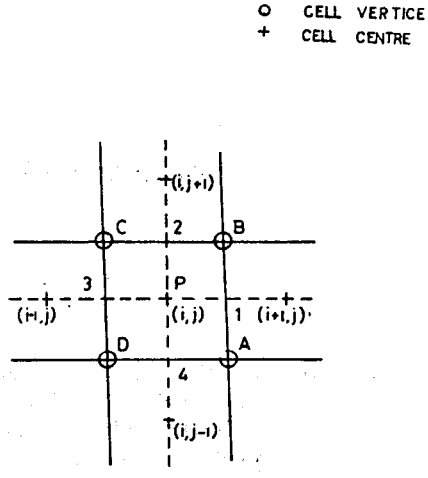

Fig. 1—Inviscid computational grid

where ΔA is the cell volume, and Q represents the net absolute flux out of the cell. The convective fluxes are calculated at the centre resulting in cell central flux balances. The contour integration of the inviscid flux vector is approximated as

$$\mathbf{Q}(\mathbf{W}_{ij})=\bar{r}\sum_{s=1}^{4}(\mathbf{F}_s\Delta r_s-\mathbf{G}_s\Delta x_s) \qquad \ldots (7)$$

where **F** and **G** are the flux vector through the sides, s. The summation is carried out over four edges of the cell as depicted in Fig. 1, and it can be simplfied as

$$\mathbf{Q}(\mathbf{W}_{ij})=\bar{r}[(\mathbf{F}_{AB}\Delta r_{AB}+\mathbf{F}_{BC}\Delta r_{BC}+\mathbf{F}_{CD}\Delta r_{CD}+\mathbf{F}_{DA}\Delta r_{DA})-(\mathbf{G}_{AB}\Delta x_{AB}+\mathbf{G}_{BC}\Delta x_{BC}+\mathbf{G}_{CD}\Delta x_{CD}+\mathbf{G}_{DA}\Delta x_{DA})] \qquad \ldots (8)$$

where $\Delta x_{BC}=(X_B-X_C)$ and $\Delta r_{AB}=(r_B-r_A)$ are incremental distances. Cell-edge value of the inviscid flux terms are approximated by the average of the two adjacent cell-centre values, for example,

$$\mathbf{F}_{AB}=\frac{1}{2}(\mathbf{F}_{i,j}+\mathbf{F}_{i+1,j}) \qquad \ldots (9)$$

The finite volume scheme Eq. (6) constructed in this manner reduces to a central-difference scheme and is second-order accurate in space provided that the mesh is smooth enough. The vector **D** is the local dissipation flux required to eliminate spurious oscillations typical to central difference algorithm.

Artificial Dissipation

The cell centred spatial discretization method is non-dissipative so that any truncation and round-off errors are not damped in time, and oscillations may be present in steady-state solution. In order to eliminate these oscillations, a dissipative term **D** is added to Eq. (6). An effective form for **D** is a blend of second and fourth order differences with coefficients depending upon the second order difference of local pressure. Specifically, let ν be defined by

$$\nu_{ij} = \left| \frac{p_{i+1,j} - 2p_{i,j} + p_{i-1,j}}{p_{i+1,j} + 2p_{i,j} + p_{i-1,j}} \right| \quad \ldots (10)$$

This quantity is second order except in regions containing a large pressure gradient. The term $\mathbf{D}_{i,j}$ is constructed so that it is third order in smooth regions of flow and first order in the vicinity of the shock wave. $\mathbf{D}_{i,j}$ has the form

$$\mathbf{D}\mathbf{U} = (\mathbf{D}_x + \mathbf{D}_r)\mathbf{U}_{i,j} \quad \ldots (11)$$

where $\mathbf{D}_x$ and $\mathbf{D}_r$ are central difference operator in i-, and j-directions, respectively. The dissipative fluxes in each direction are

$$\mathbf{D}_x\mathbf{U} = d_{i+1/2,j} - d_{i-1/2,j}$$

$$\mathbf{D}_r\mathbf{U} = d_{i,j+1/2} - d_{i,j-1/2}$$

The dissipative fluxes $d_{i+1/2,j}$ are defined as a blending of first and third difference

$$d_{1+1/2,j} = \frac{(\Delta A)_{i+1/2,j}}{\Delta t}\left(\varepsilon^{(2)}_{i+1/2,j}\Delta_x\mathbf{U}_{i,j} - \varepsilon^{(4)}_{i+1/2,j}\Delta_x^3\mathbf{U}_{i-1,j}\right) \quad \ldots (12)$$

where Δt is local time step, Δ_x is the forward difference operator given by

$$\Delta_x\mathbf{U}_{i,j} = \mathbf{U}_{i+1,j} - \mathbf{U}_{i,j}$$

The coefficient

$$\varepsilon^{(2)} = k^{(2)} \max(\nu_{i+1,j}, \nu_{i,j}) \quad \ldots (13)$$

is made proportional to ν. The other coefficient is given by

$$\varepsilon^{(2)}_{i+1/2,j} = \max\{0, (k^{(4)} - \varepsilon^{(2)}_{i+1/2,j})\} \quad \ldots (14)$$

The fourth order differences provide background dissipation throughout the computational domain but are switched off in the neighbourhood of the shock waves. The scaling $[(\Delta A_{i+1/2,j})/\Delta t]$ in Eq. (12) confirms to the inclusion of the cell volume in the dependent variables of Eq. (6). The dissipative fluxes $d_{i,j+1/2}$ and $d_{i,j-1/2}$, are calculated in an analogous manner. The typical values of the constants $k^{(2)}$ and $k^{(4)}$ are 1/4 and 1/256, respectively.

Fifth Stage Runge-Kutta Time-Stepping Scheme

Temporal integration is performed by the fifth-stage scheme[6] which is based on the Runge-Kutta method. Suppressing the subscripts (i,j), the following sequence of operations is used to obtain **U** at the time level n + 1 as:

$$\begin{aligned}
\mathbf{U}^{(0)} &= \mathbf{U}^n \\
\mathbf{U}^{(1)} &= \mathbf{U}^{(0)} - \alpha_1 \frac{\Delta t}{r_c \Delta A}(\mathbf{Q}^{(0)} - \mathbf{D}^{(0)}) \\
\mathbf{U}^{(2)} &= \mathbf{U}^{(0)} - \alpha_2 \frac{\Delta t}{r_c \Delta A}(\mathbf{Q}^{(1)} - \mathbf{D}^{(0)}) \\
\mathbf{U}^{(3)} &= \mathbf{U}^{(0)} - \alpha_3 \frac{\Delta t}{r_c \Delta A}(\mathbf{Q}^{(2)} - \mathbf{D}^{(1)}) \\
\mathbf{U}^{(4)} &= \mathbf{U}^{(0)} - \alpha_4 \frac{\Delta t}{r_c \Delta A}(\mathbf{Q}^{(3)} - \mathbf{D}^{(1)}) \\
\mathbf{U}^{(5)} &= \mathbf{U}^{(0)} - \alpha_5 \frac{\Delta t}{r_c \Delta A}(\mathbf{Q}^{(4)} - \mathbf{D}^{(1)}) \\
\mathbf{U}^{n+1} &= \mathbf{U}^{(5)}
\end{aligned} \quad \ldots (15)$$

In the above equations, the source vector **H** is included in the vector **Q**. The values of the coefficient α are as following

$$\alpha_1 = 1/4,\ \alpha_2 = 1/6,\ \alpha_3 = 3/8,\ \alpha_4 = 1/2 \text{ and } \alpha_5 = 1$$

The dissipative terms are frozen at their values in the first and third stage of the fifth stage Runge-Kutta time-stepping scheme[6] as given in Eq. (15). Thus, a considerable amount of computational time is saved by freezing the dissipative term at their values in the first and third stage. The scheme is stable for a Courant number ≤ 4. The use of the largest possible time-step at any location is allowed by the local stability bound. For most exterior aerodynamic problems a highly stretched mesh is usually employed. In such cases, the time-step is governed by the area of the smallest cell in the field. Since the cells in the far-field can be larger than the smallest one by several orders of magnitude, choosing the minimum time-step will cause a slow convergence. To avoid this difficulty, a variable time-step determined by the bound in the local Courant number is used in each zone. This destroys the time-accuracy of the

solution but accelerates convergence to the correct steady-state solution.

Boundary and Initial Conditions

The boundary conditions are enforced by using the idea of image cells at the boundaries. The flow properties are set according to the type of boundaries.

For a solid wall, the flow properties in the image cell are taken as those of the adjacent cell boundary cell, except that the normal component of the velocity is reflected to ensure the impermeability condition. The image cell is taken while applying symmetry condition in case of axisymmetric flow.

For supersonic outflow, all of the properties in the cell are extrapolated from the adjacent interior cells.

At inlet boundaries, all of the flow properties are imposed since the incoming flow is supersonic.

For transonic flow, the boundary conditions are specificed at a sufficiently large distance from the shroud.

Initially the body is assumed to be immersed completely in the uniform freestream condition.

Circumferential Pressure Distribution

The circumferential pressure distribution at angle of attack can be calculated using Newtonian type pressure distribution[4] as

$$C_p(\phi)=\frac{1}{2}[(C_{p_0}/2)^{1/2}(1+\cos\phi) + (C_{p_\pi}/2)^{1/2}(1-\cos\phi)]^2 \quad \ldots (16)$$

For small angle of attack, the Newtonian impact values are given as

$$C_{p_{0,\pi}}=2(\theta\pm\alpha)^2 \quad \ldots (17)$$

The pressure coefficient at zero angle of attack is computed using the above mentioned numerical method. The leeward and windward values of pressure coefficient $C_{p_{0,\pi}}$ can be determined using Eq. (17) and substituted in Eq. (16) to get the entire circumferential pressure distribution.

For the cone-cylinder junction, the Prandtl-Mayer formula[5] for expanding flow is given as

$$C_{p_A}=\left(C_{p_F}+\frac{2}{\gamma M_\infty^2}\right)X-\frac{2}{\gamma M_\infty^2} \quad \ldots (18)$$

where

$$X=\frac{\left(C_{p_A}+\frac{2}{\gamma M_\infty^2}\right)}{\left(C_{p_F}+\frac{2}{\gamma M_\infty^2}\right)} \quad \ldots (19)$$

where the value of C_{p_F} is known from the above mentioned numerical method.

On the cylindrical region, it is observed from the pressure distribution that the flow ceases to expand and pressure relaxes to the freestream condition. However, the recovery of the pressure will be affected by the presence of shock, expansion and compression fan and change in the geometrical shape of the launch vehicle configuration. Here, an empirical formula is used to compute pressure distribution as

$$\left(\frac{C_{p_{i-1}}}{C_{p_i}}\right)_{\alpha\neq 0}=\left(\frac{C_{p_{i-1}}}{C_{p_i}}\right)_{\alpha=0} \quad \ldots (20)$$

where i is the axial position along the body. Eqs (17), (18) and (20) can be used to calculate the complete pressure distribution on the surface of an axisymmetric spherical shaped nose-cone, cone-cylinder, cylinder with flare combination of the launch vehicle at small angle of incidence in conjunction with the above numerical method.

Once the circumferential pressure distribution at various body station have been computed, the normal load distribution can be computed by numerically integrated following expression:

$$S\frac{dCN_\alpha}{dx}=2\pi r\int_0^{2\pi} C_p(\phi)\cos\phi\, d\phi \quad \ldots (21)$$

Normal force coefficient can be evaluated as

$$CN_\alpha=\frac{\pi}{2}\int_0^L[C_{p_0}-C_{p_\pi}]r\,dx/S \quad \ldots (22)$$

where S is reference area. The centre of aerodynamic pressure can be calculated as

$$X_{CP}=\frac{\int_0^L[C_{p_0}-C_{p_\pi}]rx\,dx}{\int_0^L[C_{p_0}-C_{p_\pi}]r\,dx} \quad \ldots (23)$$

The X_{C_P} is calculated from the tip of the model.

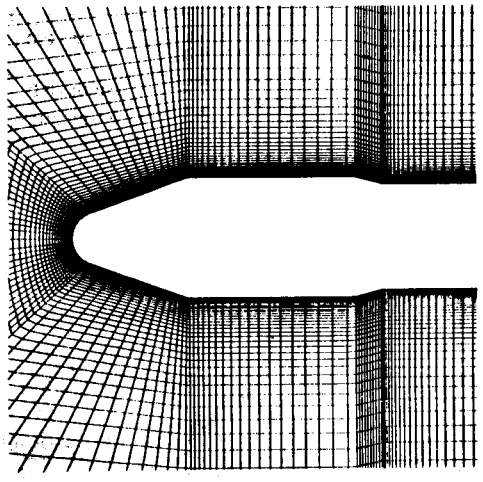

Fig. 2—Enlarged view of the gird

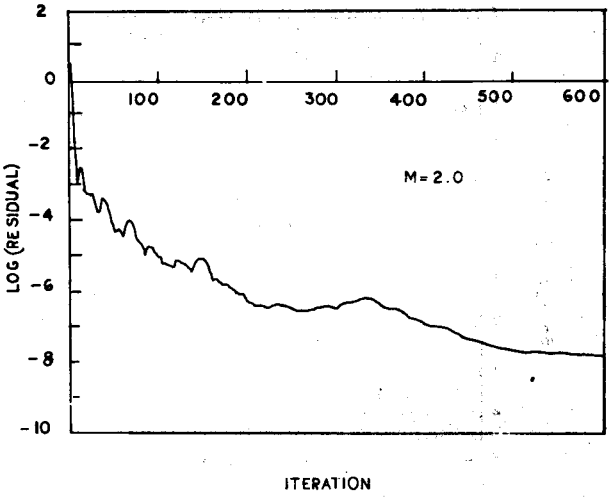

Fig. 3—Convergence history

Results and Discussion

The above numerical algorithm is used to obtain flow field over axisymmetric bulbous shaped payload of the satellite launch vehicle. Extensive numerical studies have been performed for various grid sizes. The grid size mentioned in the examples is achieved after a grid independence check. The computations were performed on LANDMARK i860 based work station. The criterion of convergence of calculated used herein is

$$|\rho^{l+1}-\rho^{l}|\leq 10^{-7}$$

where l is the iteration index. This convergence criterion is achieved in approximately 6 h of CPU time.

Bulbous payload shroud—Before proceeding to calculate pressure distributions as well as aerodynamic coefficient, an initial comparison of pressure coefficient with experimental results is performed for a typical bulbous shape heat shield, which offers dividend in terms of increase in the satellite payload volume. The forebody diameter of the model is 0.040 m, whereas the afterbody diameter is 0.035 m. The boad tail angle is 15 degree measured in the clockwise direction from the axis with reference to the coming flow direction. For the blunt nosed cone, the inclination at the forebody junction is 20 degree and the total length of the shroud from the stangnation point to the boattail is 0.083 m. These subscale dimensions were selected after considering the blockage and compatibility conditions with the model system support of the wind-tunnel. The computation is performed on 128×42 mesh points. Fig. 2 shows an enlarged view of the grid arrangement. The

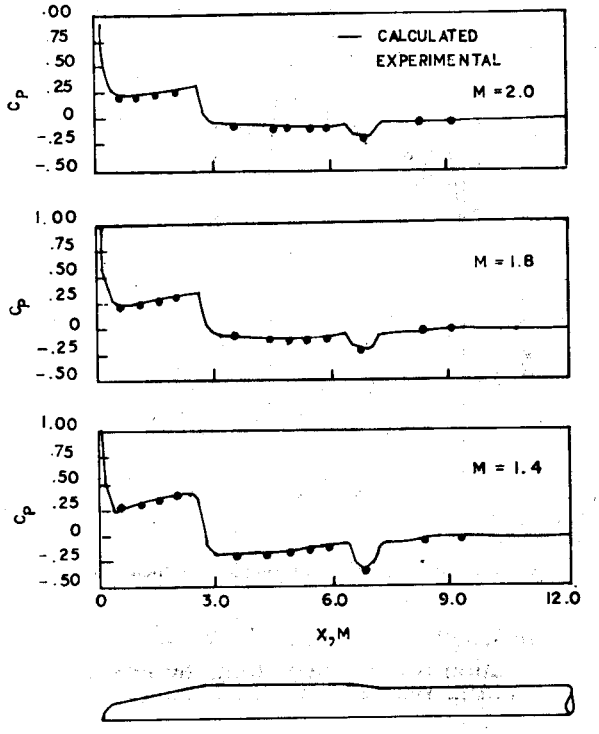

Fig. 4—Pressure distribution along the heat shield

computation was performed for freestream Mach number of 1.4, 1.8 and 2.0. Fig. 3 depicts the convergence history for $M_\infty = 2.0$. Monotonic convergence is achieved and the scheme gives an engineering acceptable solution within only 500 iterations. The surface pressure distribution is obtained along a bulbous payload shroud. The results for various freestream Mach numbers are presented in Fig. 4. The computed results agree quite well with that of the experimental data[7] along the

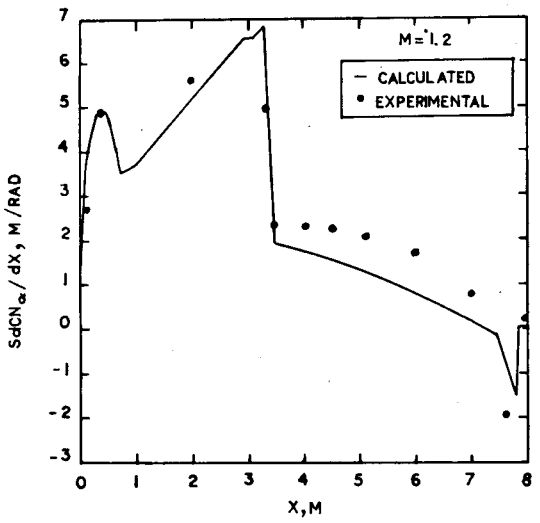

Fig. 5—Normal load distribution along the heat shield, $M = 1.2$

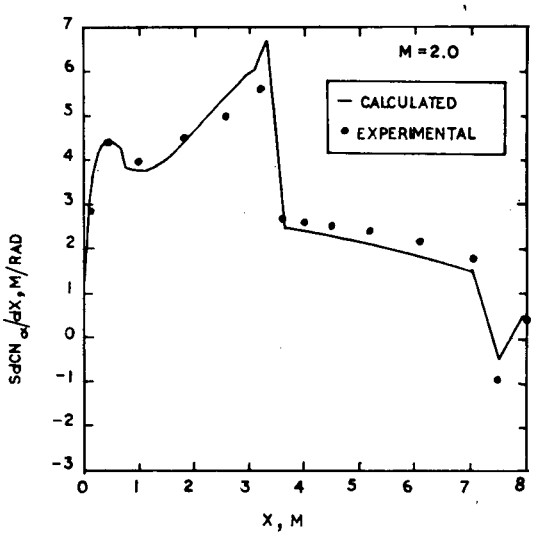

Fig. 7—Normal load distribution along the heat shield, $M = 2.0$

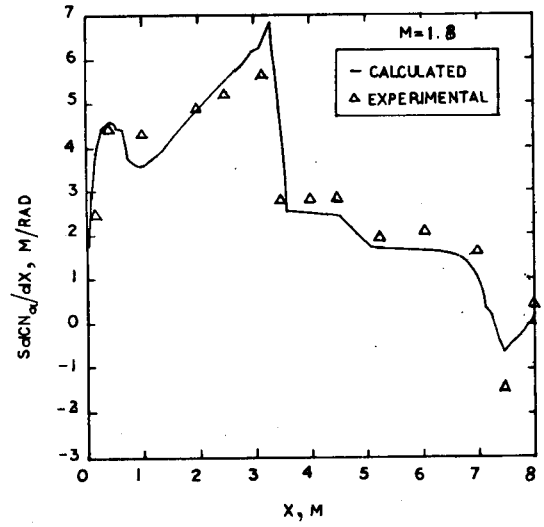

Fig. 6—Normal load distribution along theheat shield, $M = 1.8$

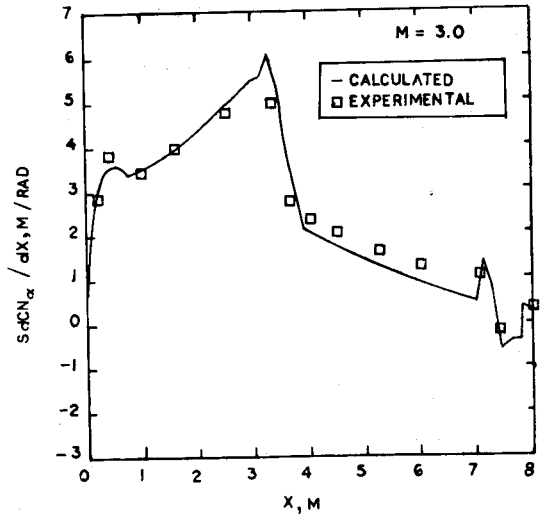

Fig. 8—Normal load distribution along the heat shield, $M = 3.0$

entire length of the heat shield. The normal load distribution is computed along the heat shield and depicted in Figs 5-8 at freestream Mach numbers range of 1.2-3.0. At $M_\infty = 1.2$, the comparison between present results with the experimental data[7] shows some disagreement on the cylindrical portion of the heat shield. This is attributed to pressure loss along the expansion fan, poor recovery of the pressure and separated flow on the boat-tail region of the heat shield. At higher supersonic free-stream Mach number, the comparison between the experimental and numerical results are reasonably in agreement execpt in the boat-tail region. This disagreement may be due to the separation of flow in the boat-tail region. The trend of the local normal load distribution are matching well with the experimental results. The values of normal force coefficient and centre of pressure are shwon in Table 1. The computed values show about ±10% error with the experimental data. This error band is within the uncertainty limit of the experimental data.

Table 1—Aerodynamic coefficient on bulbous payload shroud

Mach No.	CN_α	X_{CP}	CN_α	X_{CP}
	Experimental[7]		Calculated	
1.2	4.28	2.69	3.97	2.79
1.6	3.92	2.97	3.57	2.68

Sounding rocket—The inviscid calculations are performed for a typical sounding rocket. The configuration of the sounding rocket consisting of cone-cylinder-backward- ramp-cylinder-forward

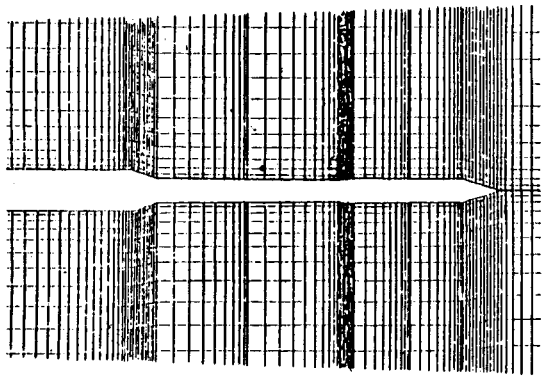

Fig. 9—Grid over sounding rocket

Table 2—Aerodynamic coefficient on sounding rocket

Mach No.	CN_α	X_{CP}	CN_α	X_{CP}
	Experimental[8]		Calculated	
2.5	0.058	8.60	0.051	8.50
3.0	0.060	8.70	0.059	8.40

ramp and cylinder. In the computation 150×42 mesh points are employed. Fig. 9 shows an enlarged view of the grid arrangement. The flow fields are obtained for freestream Mach numbers of 0.9, 1.0, 1.3 and 1.5. Fig. 10 displays the iso Mach contour at various freestream Mach numbers. The iso Mach contour plot display different flow field behaviour when the freestream Mach number changes from transonic to supersonic speed. The contour plots reveal all the essential flow field features such as expansion and compression fans. No experimental data are available to compare the computed pressure distribution with the measured data. But, the aerodynamic coefficients are measured using six components force balance in the wind-tunnel for freestream Mach numbers of 2.5 and 3.0. Table 2 gives the comparison between the present analysis with the experimental values[8], and exhibit good agreement between them.

Conclusion

A numerical algorithm is written to solve the compressible Euler equations using the fifth stage Runge-Kutta time-stepping method. The local normal load distribution is computed using the tangent-cone method in conjunction with the numerically computed axisymmetric pressure variation along the heat shield. The computed axial normal load as well as aerodynamic coefficient are compared with the available wind-tunnel data. The comparison between the present results with the experimental data shows good agreement between them at higher supersonic Mach number except in the boat tail region of the heat shield.

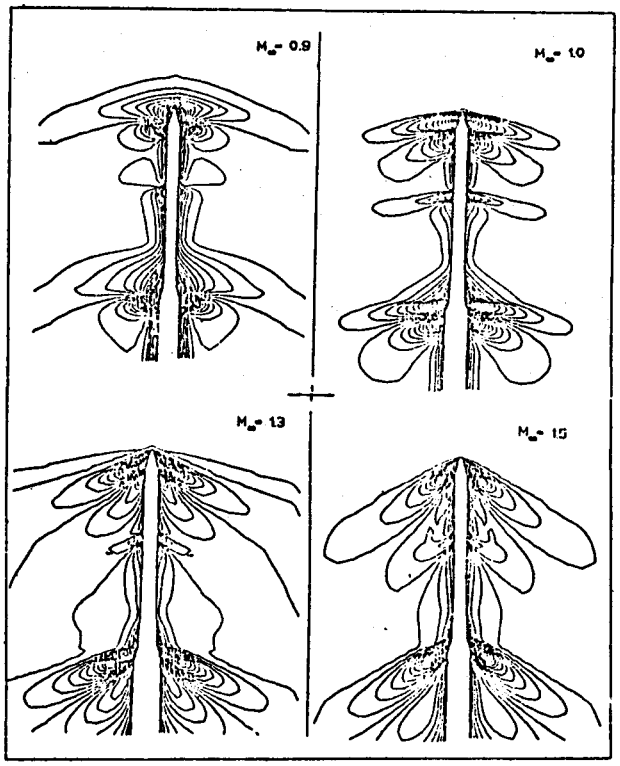

Fig. 10—Iso Mach contours plots

Nomenclature

C_p = coefficient of pressure, $(p_s - p_\infty)/q_\infty$
CN = normal force coeffient
D_{ref} = reference diameter
e = total energy
$\mathbf{F}$ = vector of x-directed fluxes
$\mathbf{G}$ = vector of r-directed fluxes
$\bar{\mathbf{H}}$ = Source vector
$\mathbf{M}$ = Mach number
p = pressure
q = dynamic pressure
S = reference surface area
t = time
T = temperature
$\mathbf{U}$ = vector of conserved variables
u, v = velocity components
X_{CP} = centre of pressure
α = static angle of attack
γ = ratio of specific heats
β = body angle
θ = roll angle
Δ = increment
ρ = density

Subscripts

0 = value of $\phi = 0$
π = value of $\phi = \pi$
∞ = freestream condition
s = surface value

References

1 Hayes W D & Probestein R F, *Hypersonic Flow Theory*, 2nd ed, Vol I, (Academic Press, New York) 1966, 522.

2 Walchner O & Clay J T, *AIAAJ*, 3(4) (1965) 752.

3 McBrayer J D, *J Spacecraft Rockets*, 3(6) (1966) 940.

4 Frberg E G & Walchner O, *AIAAJ*, 7(8) (1969) 1618.

5 Sastry M S, *J Spacecraft Rockets*, 14(8) (1977) 574.

6 Jameson A, Schmidt W & Turkel E, *Numerical Simulation of the Euler Equations by Finite Volume Methods Using Runge-Kutta Time-Stepping Schemes*, AIAA paper No 81-1259, 1981.

7 Mehta R C, *Flow field and Load computations of Heat Shield Configurations*, VSSC-ARD-25-60-Dec 91, 1991.

8 Rajendra G, Pandian S, Shivaramkrishnan A E & Varambally B S, *Force Measurements on RH-560*, National Aerospace Laboratories, Bangalore, Project Document AE 8717 Sept 1987.